

## I. FORMALISM

$$\mathcal{L}_{\text{NC}} = -2\sqrt{2}G_F \epsilon_{\alpha\beta}^{fX} (\bar{\nu}_\alpha \gamma^\mu P_L \nu_\beta) (\bar{f} \gamma_\mu P_X f) , \quad (1)$$

NC denotes the neutral current interaction with  $f \in \{e, u, d\}$ .

For chirality  $X \in \{L, R\}$ , the NSI Hamiltonian takes the form

$$H = \frac{1}{2E} U M^2 U^\dagger + \sqrt{2}G_F n_e \text{diag}(1, 0, 0) + \sqrt{2}G_F \sum_f n_f \epsilon^{fX} \quad (2)$$

We have no independent sensitivity for the chirality of  $\epsilon^X$ , so we sum over these and normalize the fermion number density  $n_f$  by the electron number density  $n_e$ . Our matter study will be wholly confined to the interior of the Earth, where we assume electrical neutrality and equal distribution of neutrons and protons, so  $n_u/n_e \simeq n_d/n_e \simeq 3$ . The effective matter NSI parameters now take the form

$$\begin{aligned} \epsilon_{\alpha\beta} &= \sum_X \sum_f \frac{n_f}{n_e} \epsilon_{\alpha\beta}^{fX} \\ &= \epsilon_{\alpha\beta}^{eV} + 3\epsilon_{\alpha\beta}^{uV} + 3\epsilon_{\alpha\beta}^{dV} \end{aligned} \quad (3)$$

We note that our definition of  $\epsilon_{\alpha\beta}$  differs from some texts, where the quark number density is used to normalize the parameters[?].

With the matter potential  $V = \sqrt{2}G_F n_e$ , we write

$$H = \frac{1}{2E} U M^2 U^\dagger + V \begin{bmatrix} 1 + \epsilon_{ee} & \epsilon_{e\mu} & \epsilon_{e\tau} \\ \epsilon_{e\mu} & \epsilon_{\mu\mu} & \epsilon_{\mu\tau} \\ \epsilon_{e\tau} & \epsilon_{\mu\tau} & \epsilon_{\tau\tau} \end{bmatrix} , \quad (4)$$

where we have assumed the components of the NSI matrix to be real.

## II. DETECTOR FORMALISM

The neutrino flux at the detector is calculated by propagating the atmospheric neutrino flux [1] through the Earth by solving the Schrödinger equation for varying density. The Earth density profile is taken from the PREM [2]. The baseline for a given trajectory is determined using an average neutrino production height of 15 km and an Earth radius of 6371 km. The propagation does not include neutrino absorption.

The oscillation probability  $P_{\alpha\beta}$  acts as a weight to the atmospheric flux, yielding the propagated flux at detector level for flavor  $\beta$  as

$$\phi_\beta^{\text{det}} = \sum_\alpha P_{\alpha\beta} \phi_\alpha^{\text{atm}} , \quad (5)$$

where we sum over the initial lepton flavors  $\alpha \in \{e, \mu, \bar{e}, \bar{\mu}\}$ . To illustrate the impact of  $\epsilon_{\mu\tau}$  on both probability and flux level, we plot the oscilloscopes resulting from Eq. 5 in Fig. ???. In the left panel, we have marked the region in which 99% of the DeepCore cascade events originating from  $\nu_e$  and  $\nu_\tau$  fluxes are contained. In the right panel, we show the two regions in which 99% of the IceCube and DeepCore track events originating from  $\nu_\mu$  fluxes are contained. Starting with the  $\nu_\mu$  flux ratio, we see that the only clear signal discernible to the IceCube detector is a flux deficiency of a factor of  $\sim 10^2$  from core-crossing neutrinos within a zenith range of  $\cos(\theta_z^{\text{true}}) > -0.87$ . DeepCore on the other hand, observes multiple fringes of flux surpluses with a factor  $\sim 10$ . The strongest surplus at 20 GeV is very weakly zenith dependent, a stark contrast to the energy-independent but zenith-sensitive IceCube deficiency. For the fluxes which drives cascades, we have to resort to the DeepCore detector alone. Here we see a somewhat weaker signal, this time a zenith-independent deficiency.

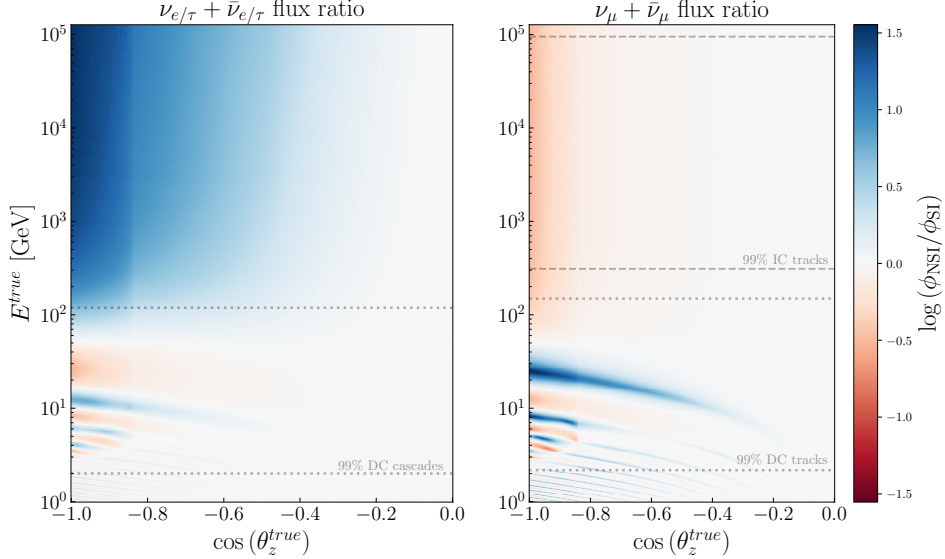


FIG. 1: Ratio of detector NSI to SI atmospheric fluxes. We set  $\epsilon_{\mu\tau} = -0.05$ , and all other  $\epsilon_{\alpha\beta} = 0$ . Within the dotted (dashed) lines, 99% of the DeepCore (IceCube) MC events are contained. Since we limit our IceCube study to muon tracks, a dashed region is omitted in the left panel.

### A. IceCube

We obtain the data from the IC-86 sterile data release [3]. The event rate for each bin reads

$$N_{ij} = T \sum_{\beta} \int_{(\cos \theta_z^r)_i}^{(\cos \theta_z^r)_{i+1}} d \cos \theta_z^r \int_{E_j^r}^{E_{j+1}^r} d E^r \int_0^\pi R(\theta^r, \theta^t) d \cos \theta^t \int_0^\infty \phi_\beta^{\text{det}} A^{\text{eff}} R(E^r, E^t) d E^t, \quad (6)$$

where  $T$  is the live time of the detector, and  $A^{\text{eff}}$  its effective area averaged over the flavors  $\beta$  from [4].  $R(x^r, x^t)$  is a resolution function, which is responsible for the smearing between the reconstructed and true parameters  $x^r$  and  $x^t$ , respectively. We assume a log-normal distribution, giving it the form

$$R(x^r, x^t) = \frac{1}{\sqrt{2\pi}\sigma_{x^r}x^r} \exp\left[-\frac{(\log x^r - \mu(x^t))^2}{2\sigma_{x^r}^2}\right]. \quad (7)$$

However, the energy reconstruction is biased [5], which means that we don't make the assumption that  $\mu(E^t) = E^r$ . To model this relationship between  $E^{true}$  and  $E^{reco}$ , we train a Gaussian process regressor on the dataset [6], from which we can extract a predicted mean and standard deviation for a given  $E^{reco}$ . We then take the  $E^{true}$  points of the 99th percentile of each distribution to obtain the limits of  $E^{true}$  at which to integrate over. We take the angular resolution function to be identically unity since the angle resolution in IceCube for track-like events is less than  $2^\circ$ , making  $\cos(\theta_z^{true})$  coincide with  $\cos(\theta_z^{reco})$  for our study.

### B. DeepCore

In this part, we use the publically available DeepCore data sample [7] which is an updated version of what was used by the IceCube collaboration in a  $\nu_\mu$  disappearance analysis [8].

The detector systematics include ice absorption and scattering, and overall, lateral, and head-on optical efficiencies of the DOMs. They are applied as correction factors using the best-fit points from the DeepCore 2019  $\nu_\tau$  appearance analysis [9].

The data include 14901 track-like events and 26001 cascade-like events, both divided into eight  $\log_{10} E^{reco} \in [0.75, 1.75]$  bins, and eight  $\cos(\theta_z^{reco}) \in [-1, 1]$  bins. Each event has a Monte Carlo weight  $w_{ijk,\beta}$ , from which we can

construct the event count as

$$N_{ijk} = C_{ijk} \sum_{\beta} w_{ijk,\beta} \phi_{\beta}^{\text{det}}, \quad (8)$$

where  $C_{k\beta}$  is the correction factor from the detector systematic uncertainty and  $\phi_{\beta}^{\text{det}}$  is defined as Eq. 5. We have now substituted the effect of the Gaussian smearing by treating the reconstructed and true quantities as a migration matrix.

The oscillation parameters used on our DeepCore simulations are from the best-fit in the global analysis in [10]:  $\theta_{12} = 33.44^\circ$ ,  $\theta_{13} = 8.57^\circ$ ,  $\Delta m_{21}^2 = 7.42 \text{ eV}^2$ , and we marginalize over  $\Delta m_{31}^2$  and  $\theta_{23}$ .

We plot the normalized event difference  $(N_{NSI} - N_{SI})/\sqrt{N_{SI}}$  where  $N_{SI}$  ( $N_{NSI}$ ) are the numbers of expected events assuming standard (non-standard) interactions in Fig. 4. This illustrates the expected sensitivity of DeepCore for the NSI parameters.

### C. PINGU

The methodology behind the PINGU simulations are the same as with our DeepCore study II B. We use the public MC [11], which allows us to construct the event count as in Eq. 8. However, since no detector systematics is yet modelled for PINGU, the correction factors  $C_{ijk}$  are all unity. As with the DeepCore data, the PINGU MC is divided into eight  $\log_{10} E^{\text{reco}} \in [0.75, 1.75]$  bins, and eight  $\cos(\theta_z^{\text{reco}}) \in [-1, 1]$  bins for both track- and cascade-like events. Just as with DeepCore, we plot the events pulls for cascades and tracks in Fig. 4. We generate ‘data’ by predicting the event rates at PINGU with the following best-fit parameters from [10], except for the CP-violating phase which is set to zero for simplicity.

$$\begin{aligned} \Delta m_{21}^2 &= 7.42 \times 10^{-5} \text{ eV}^2, \quad \Delta m_{31}^2 = 2.517 \times 10^{-3} \text{ eV}^2, \\ \theta_{12} &= 33.44^\circ, \quad \theta_{13} = 8.57^\circ, \quad \theta_{23} = 49.2^\circ, \quad \delta_{\text{CP}} = 0. \end{aligned} \quad (9)$$

## III. RESULTS

### A. Methodology

For our analyses, we define our  $\chi^2$  as

$$\chi^2(\hat{\theta}, \alpha, \beta, \kappa) = \sum_{ijk} \frac{(N_{ijk}^{\text{th}} - N_{ijk}^{\text{data}})^2}{\left(\sigma_{ijk}^{\text{data}}\right)^2 + \left(\sigma_{ijk}^{\text{syst}}\right)^2} + \frac{(1-\alpha)^2}{\sigma_{\alpha}^2} + \frac{\beta^2}{\sigma_{\beta}^2} \quad (10)$$

where we minimize over the model parameters  $\hat{\theta} \in \{\Delta m_{31}^2, \theta_{23}, \epsilon\}$ , the penalty terms  $\alpha$  and  $\beta$ , and the free parameter  $\kappa$ .  $N_{ijk}^{\text{th}}$  is the expected number of events from theory, and  $N_{ijk}^{\text{data}}$  is the observed number of events in that bin. We set  $\sigma_{\alpha} = 0.25$  as the atmospheric flux normalization error, and  $\sigma_{\beta} = 0.04$  as the zenith angle slope error [1]. The observed event number has an associated Poissonian uncertainty  $\sigma_{ijk}^{\text{data}} = \sqrt{N_{ijk}^{\text{data}}}$ . For IceCube, the event count takes the form

$$N_{ijk}^{\text{th}} = \alpha [1 + \beta(0.5 + \cos(\theta_z^{\text{reco}})_i)] N_{ijk}(\hat{\theta}), \quad (11)$$

with  $N_{ijk}(\hat{\theta})$  from Eq. 6. Here, we allow the event distribution to rotate around the median zenith angle of  $\cos(\theta_z^{\text{reco}}) = -0.5$ .

For DeepCore and PINGU, and the event count takes the form

$$N_{ijk}^{\text{th}} = \alpha [1 + \beta \cos(\theta_z^{\text{reco}})_i] N_{ijk}(\hat{\theta}) + \kappa N_{ijk}^{\mu_{\text{atm}}}, \quad (12)$$

with  $N_{ijk}(\hat{\theta})$  from Eq. 8.  $N_{ijk}^{\mu_{\text{atm}}}$  is the muon background, which is left to float freely in the DeepCore analysis. The background at PINGU can be considered negligible to first order [11], and we thus put  $\kappa = 0$  when calculating the PINGU  $\chi^2$ . Since the median zenith is  $\cos(\theta_z^{\text{reco}}) = 0$  for DeepCore and PINGU, we allow the event count to rotate around zero.

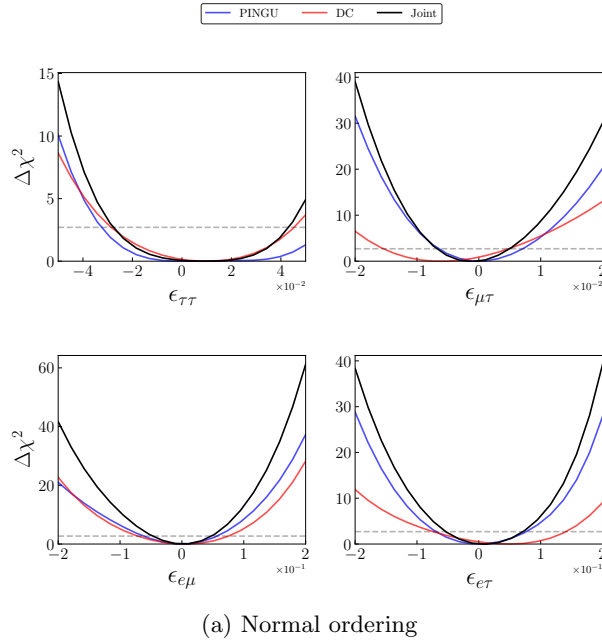


FIG. 2: Expected  $\Delta\chi^2$  after three years of data.  $\Delta m_{31}^2$  and  $\theta_{23}$  and have been marginalized out, and all other NSI parameters other than the one shown in each panel are fixed to zero.

We treat the uncorrelated systematic uncertainties differently for each detector. For IceCube, we set  $\sigma_{ijk}^{\text{syst}} = f\sqrt{N_{ijk}^{\text{data}}}$ . We consider (best) worst-case scenarios in IceCube assuming ( $f = 5\%$ ),  $f = 15\%$ . For PINGU, we use the same form but instead assume  $f = 0\%$  and  $f = 5\%$  for the best and worst-cases respectively. For DeepCore, we use the provided systematic error distribution which accounts for uncertainties in the finite MC statistics and in the data-driven muon background estimate [7].

### B. Constraining the NSI parameters

First, we set all standard oscillation parameters to their current best-fit values of Eq. 9, except for  $\Delta m_{31}^2$  and  $\theta_{23}$ , which we marginalize over their  $3\sigma$  ranges of  $2.435 \times 10^{-3}$  to  $2.598 \times 10^{-3}$  eV<sup>2</sup> and  $40.1$  to  $51.7^\circ$  respectively. After the oscillation parameters have been marginalized out, we plot  $\Delta\chi^2$  for each of the four NSI parameters in Fig. 2. We record the confidence levels in Table. ?? and best-fit points in Table III.

We can explain the asymmetry by looking at the oscillogram of the ratio  $P(\epsilon_{\mu\tau}^-)/P(\epsilon_{\mu\tau}^+)$  in Fig. ??, which is the  $P_{\mu\mu}$  survival probability given  $\epsilon_{\mu\tau} = -0.05$  divided by  $P_{\mu\mu}$  for  $\epsilon_{\mu\tau} = 0.05$ . Muon events are the most abundant in IceCube and DeepCore/PINGU, and it suffices to study  $P_{\mu\mu}$  to explain the asymmetry. We see that positive  $\epsilon_{\mu\tau}$  generates a slightly higher  $P_{\mu\mu}$  for energies around 20 GeV (pink area), while negative  $\epsilon_{\mu\tau}$  produces higher  $P_{\mu\mu}$  for almost all other combinations of  $E^{\text{true}}$ ,  $\cos(\theta_z^{\text{true}})$ . As we see in the flux ratio plot, this muon survival abundance is indeed preserved at flux level.

As we see in Fig. 3, the binned PINGU event count for  $\epsilon_{\mu\tau} = -0.02$  outnumber the event count with  $\epsilon_{\mu\tau} = 0.05$  for all bins except one, giving a high  $\Delta\chi^2$  on both sides and slightly higher for  $\epsilon_{\mu\tau} = -0.02$ . DeepCore on the other hand, has no bins where the event count for  $\epsilon_{\mu\tau} = -0.02$  surpasses the event count for  $\epsilon_{\mu\tau} = +0.02$ , giving weak statistics for the negative side.

Comparing the PINGU results in Fig. ?? and the DeepCore results in Fig. ??, we note that the best-fit for each NSI parameter for the PINGU experiment is expected to be zero. This is because the ‘data’ we generated during the PINGU simulations assumes no NSI since they have yet to be observed in nature. This introduces a non-NSI bias in our joint analysis, since PINGU has stronger statistics than DeepCore, and will thus pull the joint  $\chi^2$  towards  $\epsilon = 0$ .

For the joint analysis, we follow the parameter goodness-of-fit prescription [12] and construct the joint  $\chi^2$  as

$$\chi_{\text{joint}}^2 = \chi_{\text{IC}}^2 + \chi_{\text{DC}}^2 + \chi_{\text{P}}^2 - \chi_{\text{IC},\min}^2 - \chi_{\text{DC},\min}^2 - \chi_{\text{P},\min}^2 \quad (13)$$

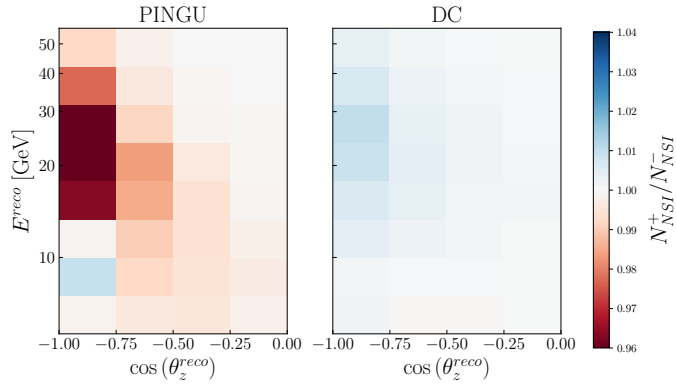


FIG. 3: The best-fit event count ratio at each detector for negative and positive  $\epsilon_{\mu\tau}$ . PINGU shows promising of distinguishing the sign of  $\epsilon_{\mu\tau}$ , but favoring  $\epsilon_{\mu\tau} < 0$  while DeepCore has higher statistics for  $\epsilon_{\mu\tau} > 0$  and a poor distinction for  $\epsilon_{\mu\tau} < 0$

Parameter	Best 90% CL	Best $3\sigma$	Worst 90% CL	Worst $3\sigma$
IceCube				
$\epsilon_{\mu\tau}$	[-0.0098, 0.009]	[-0.0148, 0.014]	[-0.0152, 0.0145]	[-, -]
DeepCore				
$\epsilon_{\tau\tau}$	[-0.029, 0.045]	[-, -]	[-0.029, 0.045]	[-, -]
$\epsilon_{\mu\tau}$	[-0.015, 0.0048]	[-, 0.015]	[-0.015, 0.0048]	[-, 0.015]
$\epsilon_{e\mu}$	[-0.072, 0.075]	[-0.132, 0.127]	[-0.072, 0.075]	[-0.132, 0.127]
$\epsilon_{e\tau}$	[-0.074, 0.141]	[-0.174, 0.20]	[-0.074, 0.141]	[-0.174, 0.20]
IceCube + DeepCore				
$\epsilon_{\mu\tau}$	[-0.0182, 0.00030]	[-, 0.0104]	[-0.0185, 0.00030]	[-, 0.0104]

TABLE I: IceCube and DeepCore results from the  $\Delta\chi^2$  in Fig. 2. IceCube best and worst case refers to the systematic uncertainty scenarios considered as in Sec. III A

with test statistic  $\chi^2_{\text{joint,min}}$ . The results are shown in Fig. 2a and summarized in Table ??.

Parameter	Best 90% CL	Best $3\sigma$	Worst 90% CL	Worst $3\sigma$
PINGU				
$\epsilon_{\tau\tau}$	[-0.0326, -]	[-0.0482, ]	[-0.0371, -]	[-, -]
$\epsilon_{\mu\tau}$	[-0.0065, 0.0071]	[-0.011, 0.013]	[-0.0078, 0.0087]	[-0.0136, 0.0162]
$\epsilon_{e\mu}$	[-0.062, 0.057]	[-0.122, 0.103]	[-0.1057, 0.0799]	[-0.198, 0.141]
$\epsilon_{e\tau}$	[-0.069, 0.077]	[-0.121, 0.133]	[-0.1072, 0.1022]	[-0.1805, 0.1633]
DeepCore + PINGU				
$\epsilon_{\tau\tau}$	[-0.028, 0.043]	[-0.043, -]	[-0.0285, 0.0423]	[-0.0447, -]
$\epsilon_{\mu\tau}$	[-0.0067, 0.0049]	[-0.0109, 0.0101]	[-0.0049, 0.0086]	[-0.0098, 0.0146]
$\epsilon_{e\mu}$	[-0.048, 0.048]	[-0.090, 0.085]	[-0.0721, 0.0503]	[-0.1262, 0.0931]
$\epsilon_{e\tau}$	[-0.053, 0.072]	[-0.101, 0.118]	[-0.0901, 0.0624]	[-0.1491, 0.1168]
IceCube + DeepCore + PINGU				
$\epsilon_{\mu\tau}$	[-0.0088, 0.003]	[-0.0128, 0.0081]	[-0.01, 0.0028]	[-0.0145, 0.0087]

TABLE II: PINGU and joint results from the  $\Delta\chi^2$  in Fig. 2. PINGU best and worst cases refers to the systematic uncertainty scenarios considered as in Sec. III A

Parameter	Best fit		
	$\Delta m_{31}^2$	$\theta_{23}$	$\epsilon$
DeepCore			
$\epsilon_{\tau\tau}$	2.435	47.84	0.0125
$\epsilon_{\mu\tau}$	2.435	43.97	-0.005
$\epsilon_{e\mu}$	2.435	43.97	0
$\epsilon_{e\tau}$	2.435	43.97	0.05
IceCube			
$\epsilon_{\mu\tau}$	2.435	51.70	0
IceCube + DeepCore			
$\epsilon_{\mu\tau}$	2.517	43.97	-0.01

TABLE III: Best fit points for  $\Delta m_{31}^2$  and  $\theta_{23}$  are given in units of  $10^{-3}\text{eV}^2$  and degrees, respectively.

- 
- [1] M. Honda et al., Calculation of atmospheric neutrino flux using the interaction model calibrated with atmospheric muon data. doi:10.1103/PhysRevD.75.043006.
  - [2] A. M. Dziewonski and D. L. Anderson, Preliminary reference Earth model 25 (4) 297–356. doi:10.1016/0031-9201(81)90046-7.
  - [3] M. G. Aartsen et al., Searching for eV-scale sterile neutrinos with eight years of atmospheric neutrinos at the IceCube Neutrino Telescope 102 (5) 052009. doi:10.1103/PhysRevD.102.052009.
  - [4] IceCube Collaboration, All-sky point-source IceCube data: Years 2010–2012. doi:10.21234/B4F04V.
  - [5] C. Weaver, Evidence for Astrophysical Muon Neutrinos from the Northern Sky 149.
  - [6] IceCube Collaboration, Search for sterile neutrinos with one year of IceCube data. URL <https://icecube.wisc.edu/data-releases/2016/06/search-for-sterile-neutrinos-with-one-year-of-icecube-data/>
  - [7] IceCube Collaboration, Three-year high-statistics neutrino oscillation samples. doi:10.21234/ac23-ra43.
  - [8] IceCube Collaboration et al., Measurement of Atmospheric Neutrino Oscillations at 6–56 GeV with IceCube DeepCore 120 (7) 071801. doi:10.1103/PhysRevLett.120.071801.
  - [9] IceCube Collaboration 1 et al., Measurement of atmospheric tau neutrino appearance with IceCube DeepCore 99 (3)

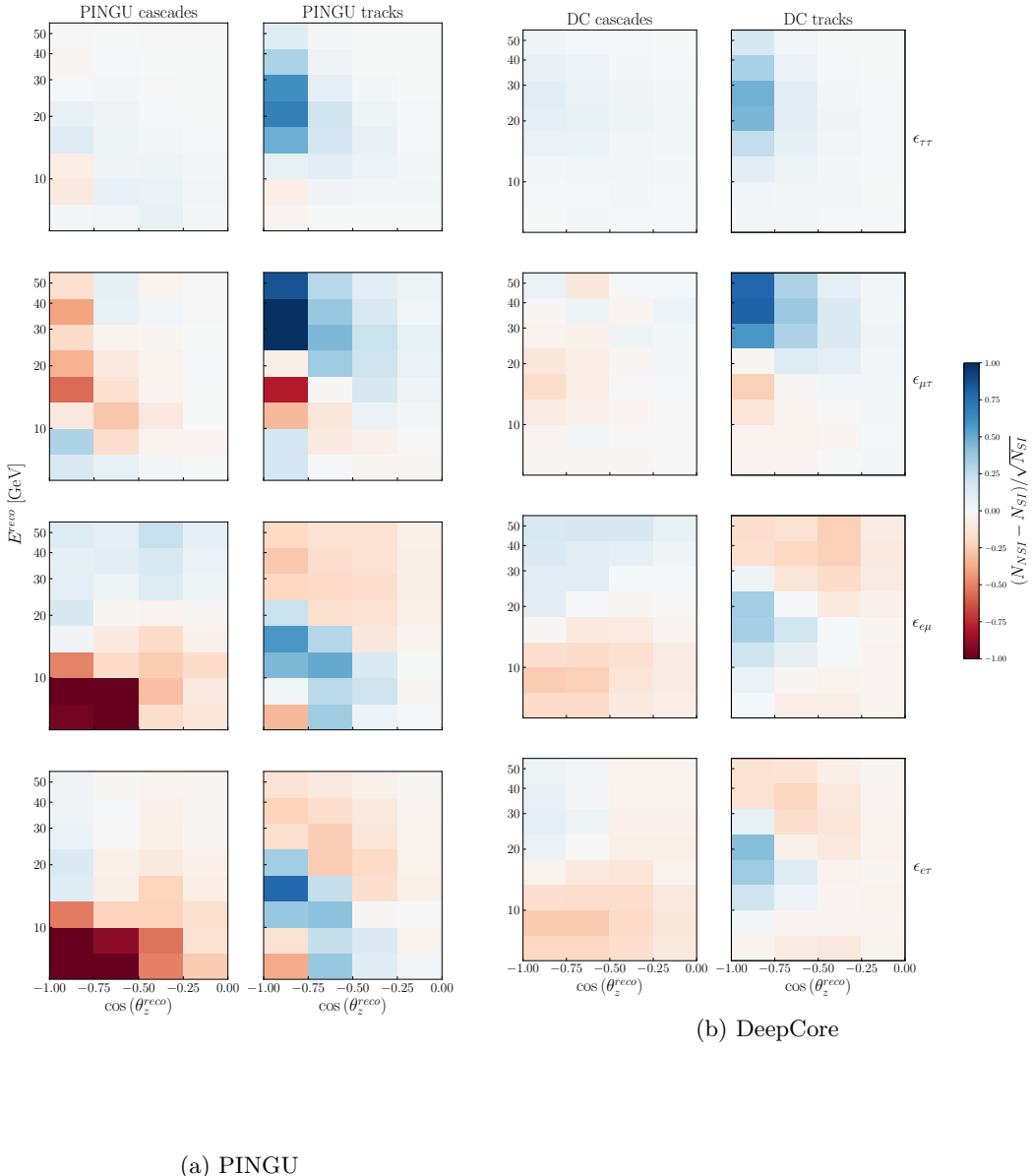
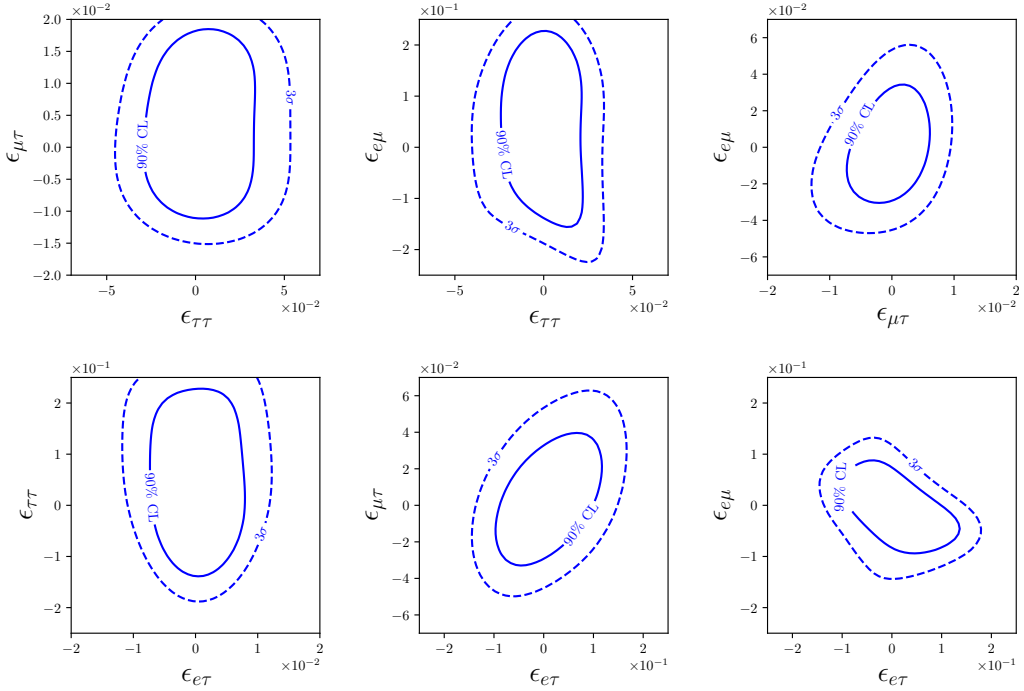


FIG. 4: Expected pulls of the form  $(N_{NSI} - N_{SI})/\sqrt{N_{SI}}$  for PINGU and DeepCore after 3 years. We compare the NSI event count with  $\epsilon_{\mu\tau} = -0.01$  to the standard interaction count

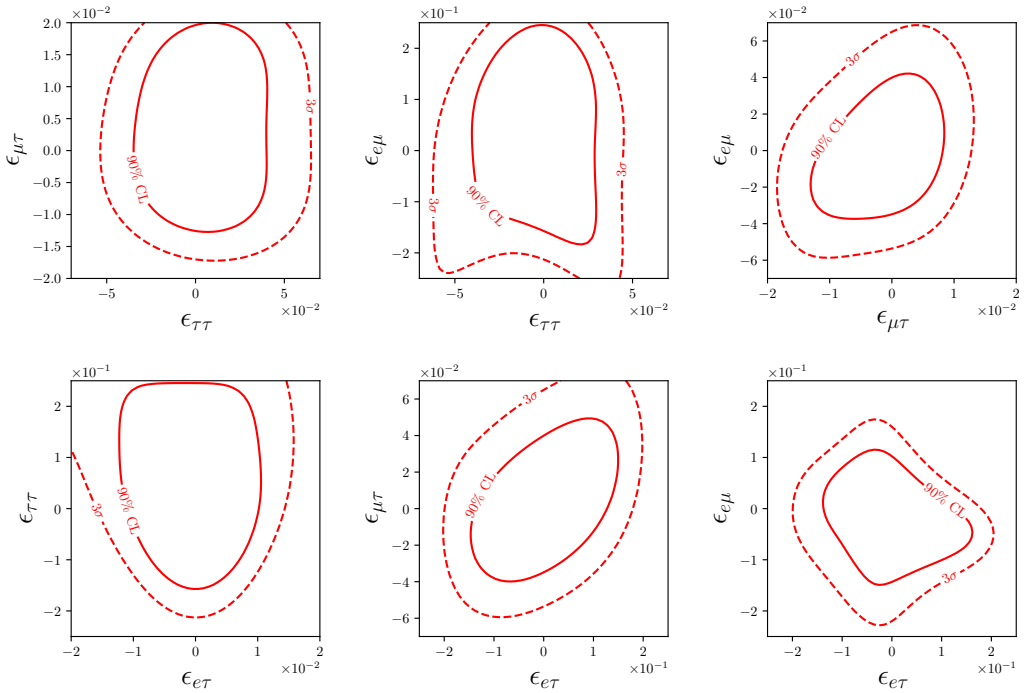
032007. doi:10.1103/PhysRevD.99.032007.

- [10] I. Esteban et al., The fate of hints: Updated global analysis of three-flavor neutrino oscillations 2020 (9) 178. doi: 10.1007/JHEP09(2020)178.
- [11] IceCube Collaboration, IceCube Upgrade Neutrino Monte Carlo Simulation. doi:10.21234/qfz1-yh02.
- [12] M. Maltoni and T. Schwetz, Testing the statistical compatibility of independent data sets 68 (3) 033020. arXiv:hep-ph/0304176, doi:10.1103/PhysRevD.68.033020.

$f = 0\%$



$f = 5\%$



DeepCore (2017)	Demidov (2020) DC analysis	This DC+PINGU analysis
✓ Honda atmospheric fluxes	✓ Honda atmospheric fluxes	✓ Honda atmospheric fluxes
✗ Only look at tracks and $\epsilon_{\mu\tau}$	✓ Looks at tracks + cascades for $\epsilon_{\mu\tau}$ and $\epsilon_{\tau\tau}$	✓ Tracks and cascades for all flavors
✗ DC Monte Carlo from an older dataset	✓ Data and Monte Carlo from DC 2018	✓ Reco $\rightarrow$ true mapping from Monte Carlo migration matrix
✗ 8 E bins from $6.3 \text{ eV}^2$ to $56 \text{ eV}^2$	✓ 8 E bins from $5.6 \text{ eV}^2$ to $56 \text{ eV}^2$	✓ 8 E bins from $5.6 \text{ eV}^2$ to $56 \text{ eV}^2$
✗ 8 z bins from -1 to 0	✓ 8 z bins from -1 to 1	✓ 8 zenith angle bins from -1 to 1
✗ Use "Overall" and "relative $\nu_e$ to $\nu_\mu$ " normalization	✗ Use "Overall" and "relative $\nu_e$ to $\nu_\mu$ " normalization	✓ Flux normalization uncertainty of 25%
✗ Prior on spectral index	✗ Prior on spectral index	✓ Zenith angle uncertainty of 4%
✗ No zenith angle normalization	✗ No zenith angle normalization	✓ No priors on oscillation parameters
✓ No priors on $\Delta m_{31}^2, \theta_{23}, \theta_{13}$	✓ No priors on $\Delta m_{31}^2, \theta_{23}$	✓ Marginalize $\Delta m_{31}^2$ and $\theta_{23}$ . All other oscillation parameters are fixed.
	✓ Fixes $\Delta m_{21}^2, \theta_{12}, \theta_{13}$	
	✗ Uncertainty on hadron production in atmosphere	
	✗ Uncertainty on neutrino nucleon cross section	